Computers & Geosciences 88 (2016) 97–114

Contents lists available at ScienceDirect

Computers & Geosciences

journal homepage: www.elsevier.com/locate/cageo

Case study

A descriptive study of fracture networks in rocks using complex network metrics

Elizabeth Santiago [a,*], Jorge X. Velasco-Hernández [a], Manuel Romero-Salcedo [b]

[a] Instituto de Matemáticas, UNAM Campus Juriquilla, Boulevard Juriquilla 3001, Juriquilla, Querétaro CP 76230, Mexico
[b] Programa de Matemáticas Aplicadas y Computación, Instituto Mexicano del Petróleo, Av. Eje Central Lázaro Cárdenas Norte, 152. Col. San Bartolo Atepehuacan, Mexico-city CP 07730, Mexico

ARTICLE INFO

Article history:
Received 26 May 2015
Received in revised form
24 December 2015
Accepted 29 December 2015
Available online 31 December 2015

Keywords:
Fracture networks
Complex networks
Centrality measures
Communicability
Topology of networks

ABSTRACT

In this paper we describe the static topological fracture structure of five rock samples from three regions in Eastern Mexico by the application of centrality and communicability measures used in the area of complex networks. The information obtained from fracture images is used to characterize the fracture networks. The analysis is divided into two groups of characteristics. The first provides a general summary of the fracture network through the description of the number of nodes, edges, diameter, radius, lengths and clustering coefficients. A second group of features centers on the description of communicability in the network by means of three indexes recently proposed. In addition, we apply centrality measures (betweenness, closeness, eigenvector and eccentricity) for quantifying the importance of nodes in the entire network. Finally, we identify a topology for fracture networks using a classification based on the degree of communicability. The most important results obtained in this work are focused in the topological characteristic patterns found in fracture networks applying the approach of complex networks that in general provide local and global parameters of connectivity and communicability.

1. Introduction

Fracture systems have a large impact on fluid flow and, therefore, a crucial influence on the productivity of geological formations especially in those of low permeability. Rock fracture systems have attracted much attention for a long time in fields such as hydrocarbon geology and hydrogeology (Cacas et al., 1990; Caine et al., 1996; Escuder-Viruete et al., 2003; Hitchmough et al., 2007; Narr et al., 2006; Sarda et al., 2002; Sarkar et al., 2004). Analysis for rock fracture systems is necessary in the evaluation of potential oil production in reservoirs (Bogatkov and Babadagli, 2007; Han et al., 2013; Hansford and Fisher, 2009; Witte et al., 2012). It is traditionally centered in the determination of fracture lengths, orientations, apertures, intensity and permeability; see for example (Dershowitz and Herda, 1992; Hakami and Larsson, 1996; Lee et al., 2011; Rouleau and Gale, 1985; Smith and Schwartz, 1984; Voeckler and Allen, 2012; Koike et al., 2015). In nature fracture networks are in 3D, and it is hard to study them from fracture networks in 2D only. In addition, fracture flow capability not only depends on the geometry and topology of the channel systems but also on other parameters such as viscosity, pressure gradient, rugosity of the surface (Berkowitz, 2002; Ghaffar et al., 2012). Nevertheless, in geological scenarios the analysis in 2D images can be useful in order to identify geometric and topological parameters that can support the characterization of the rock samples (Jafari and Babadagli, 2012; Santiago et al., 2012; Sarkar et al., 2004). In this work, we characterize the static properties in 2D fracture networks though which a fluid may flow in order to identify topological properties that may become important in conductive fractures.

Recent contributions in the study of fracture characterization are, for example, Lyman (2003), Santiago et al. (2014), Seetal and Natarajan (2010) and Wang et al. (2011). In particular, works focused in the topological analysis of 2D fracture systems that apply classical graph theory are reported (Andresen et al., 2013; Bour and Davy, 1998; Hardebol and Bertotti, 2013; Sanderson and Nixon, 2015; Santiago et al., 2014; Yang et al., 1995). These authors focus on computer image processing tools, techniques for extracting the rock fracture system from images, fracture tracing, extraction of features of fractures such as length, width, spacing, density, roughness, aperture and determination of orientations, detection and quantification of cross and ending points of the fractures, and in general computation of distributions of all of these attributes. In previous works (Santiago et al., 2012, 2014) a methodology is proposed for the identification of regions of

* Corresponding author.
E-mail addresses: esantigo@im.unam.mx (E. Santiago), jx.velasco@im.unam.mx (J.X. Velasco-Hernández), mromeros@imp.mx (M. Romero-Salcedo).

http://dx.doi.org/10.1016/j.cageo.2015.12.021
0098-3004/

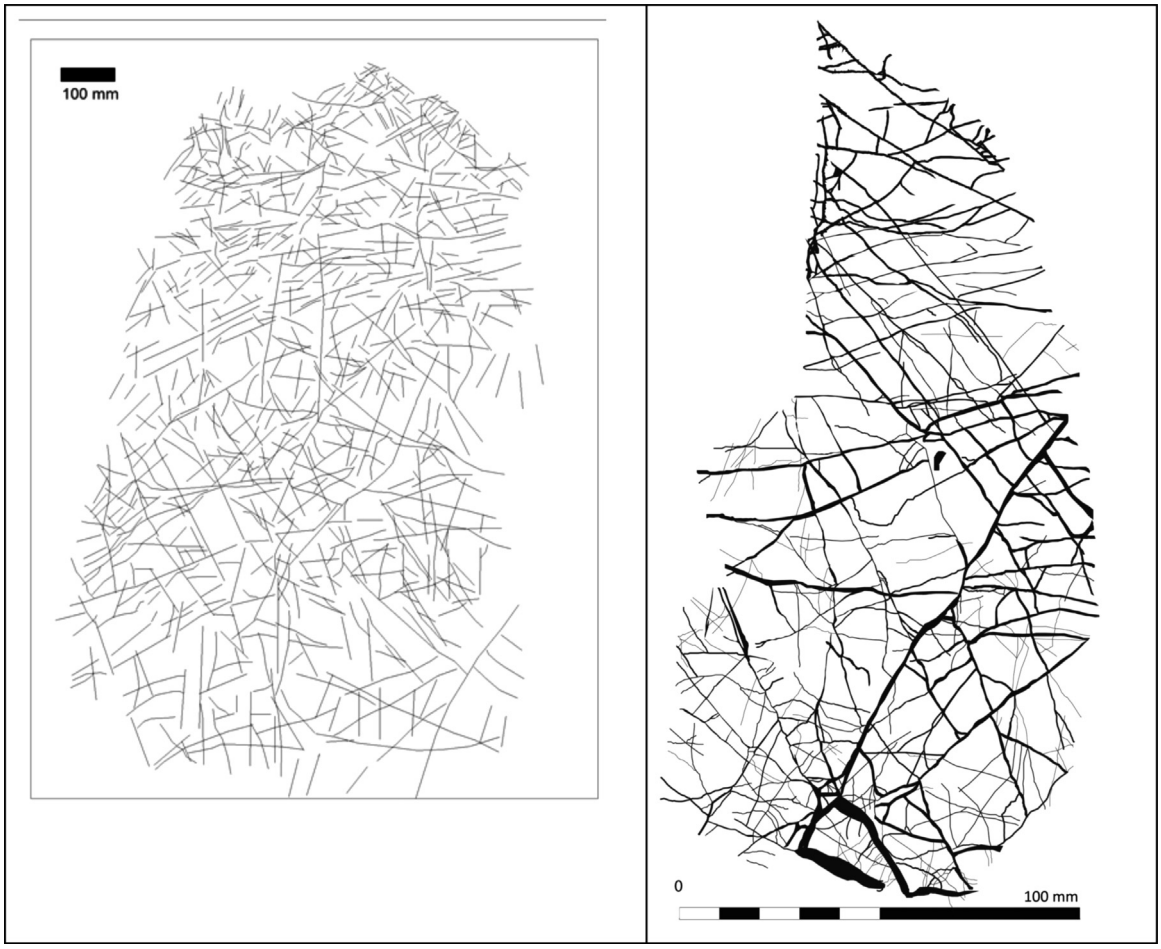

Fig. 1. Samples of original fracture networks. (Left) Sample of fractures JT-6 with number of nodes and links of 663 and 728, respectively. (Right) Sample of fractures MM with number of nodes and links of 1567 and 1996, respectively. A scale bar (mm) is included on each figure.

interest through a preprocessing of fracture images in rocks. Noise removal and filtering are applied to enhance the image quality and to facilitate further processing, where the rock fracture system is obtained after transforming it into a binary image.

In this work, for the analysis of the fractures in rocks, we use information from two-dimensional binary images where connected multiple fractures form a network. The five samples of rocks we analyze come from three different locations of South-Eastern Mexico, one of them (MM) comes from an outcrop (Jurassic–Early Cretaceous) located in Xochitlán, Chiapas; the sample labeled with CH-2 comes from the Northern Golf of Mexico (Paleocene-Eocene), and samples JT-3, JT-6 and JT-8 (Tithonian) are belonging to the Campeche region. These samples are studied due to the interest of characterizing naturally fracture reservoirs; and all these samples come from naturally fractured rocks except CH-2 that corresponds to a clayey-sandstone reservoir. Depending on the nature of the rock fracture system (cores, outcrops, hand-samples), the revealed structures have significant heterogeneity (Baker and Kuppe, 2000). Knowledge of the topological structural properties of such fracture systems may provide useful information for understanding their organization, function and dynamics. For establishing the relation between insights gained from this study and the fracture features that modelers need (Dershowitz and Herda, 1992; Lee et al., 2011), we characterize topological properties of the fracture networks by using quantitative measures used in complex network (Estrada, 2010a; Newman, 2003, 2010) in order to find distinctive patterns that modelers could use in practice. Furthermore, a topological approach that classifies networks in four classes is applied to fracture networks that is essentially based on local and global communicability. One of the most common indicators for identifying the most important nodes within the network is the centrality of a graph or network, and in this work, a set of centrality measures is applied and all of them are correlated themselves. Three of such measures stand out as important: closeness, betweenness, and eigenvector centrality (Bonacich, 1987; Freeman, 1977; Sabidussi, 1966).

The organization of the document is presented as follows. In Section 2, a fracture network is defined as a complex network describing its main elements. In Section 3, the images of fracture networks used are presented, first showing the original sources of fracture images, and then displaying them as graphs; also in this section, the methods and formulations of metrics applied are described. In Section 4, the results of the application of centrality and communicability measures and the relations among them are presented. The method for identify the topological class for fracture networks is also described in this section; and finally, in Section 5, we comment our conclusions and relevant points.

2. Fracture networks as complex networks

In general, a network is defined as a tuple $G=(V,E)$, where V is a finite set of nodes, and E is a relation between nodes. In an undirected graph, the relation is symmetric, that is, the links are bidirectional, and it is named unweighted graph when the value of connection is one if there is a relation between two nodes and

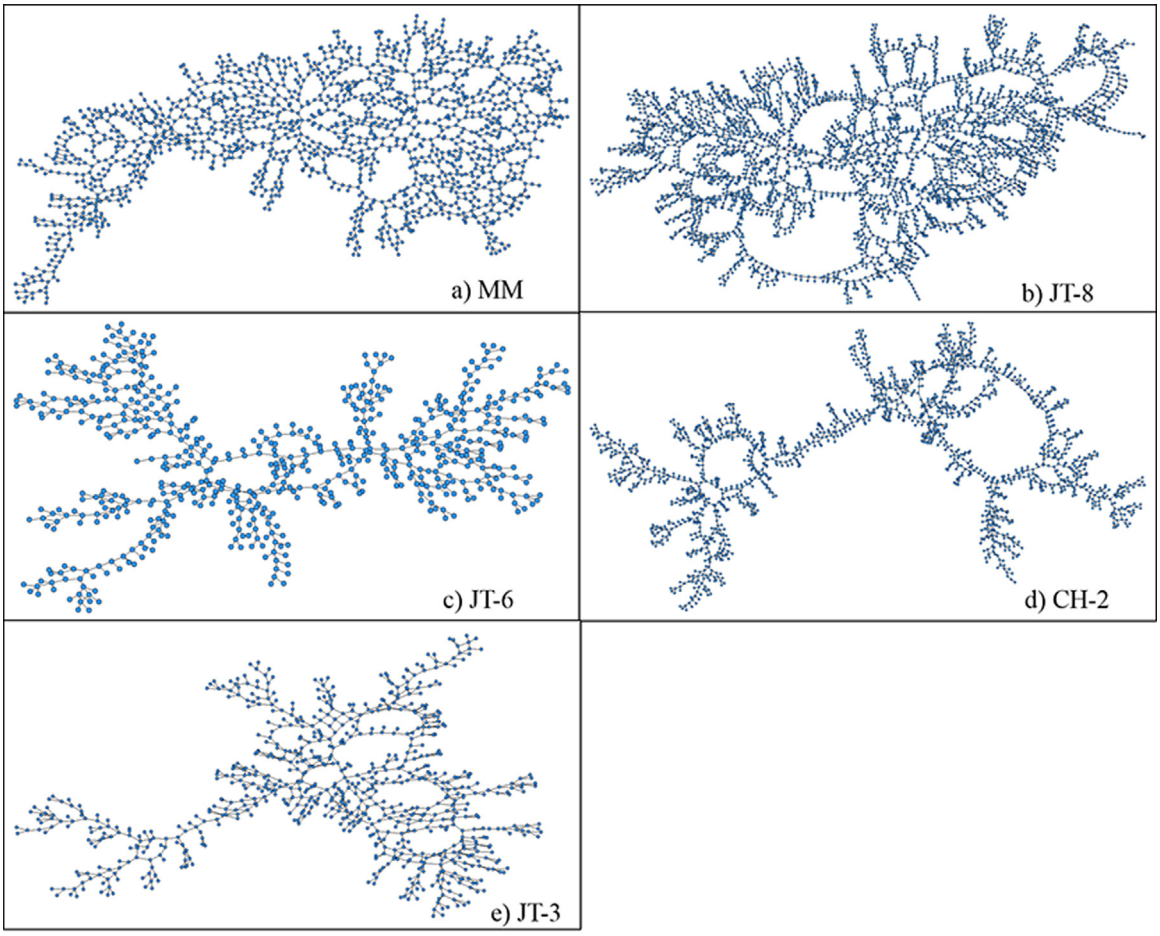

Fig. 2. Examples of extracted fracture networks using Ucinet for your representations. The representation of each network is projected so that avoids the nodes overlap each other and optimizes space among nodes.

otherwise zero. Defining a fracture network as G, the set V of nodes represents the intersection points of the fracture segments, and the set E of edges represents links or connections between intersection points. In this work, we define the fracture networks as connected, undirected and unweighted graphs and denote as $n=|V|$ and $m=|E|$ the number of nodes and edges or links, respectively. $d_g(s, t)$ is the length of a path between the nodes s and t; the subindex g indicates that it is the geodesic path (the shortest path). The connectivity of nodes and edges is given by the adjacency matrix A, it contains only zeros and ones. Once this matrix is determined from the fracture image, the centrality measures and topological indices are computed, namely betweenness, closeness, eigenvector centrality, eccentricity, invariability and the Estrada index, all of them are described in Appendix A.

Table 1
Summary of characteristics of fracture networks.

Sample	n	m	Size (n/m)	D	r	$\overline{C}$	T	M
JT-8	3585	4183	0.857	111	57	0.046	135	4353
CH-2	1686	1905	0.885	124	62	0.066	76	2669
MM	1567	1996	0.785	94	47	0.054	68	2045
JT-3	779	887	0.878	51	26	0.026	16	1239
JT- 6	633	728	0.869	51	26	0.065	26	1590

Description of parameters:
n=number of nodes, m=number of links, D=diameter, r=radius, $\overline{C}$=clustering coefficient, and T=number of triangles, M=total number of fracture segments.

3. Method

3.1. Data processing

The data used in this work come from fracture images with different file extensions (png, bmp). Two examples of original images corresponding to fractures in rocks are shown in Fig. 1. Other three of the samples used are similar to the traces displayed on the left side in Fig. 1 that are JT-3, JT-8 and CH-2 (see Figs. B.1–B.3 in Appendix B), the sizes of these fracture images are in average $0.80 \times 0.80\ \text{cm}^2$; while the size of the sample on the right side in Fig. 1, is $10 \times 20\ \text{cm}^2$ approximately. For the image processing and algorithms to construct the fracture segments see Santiago et al. (2012). The resulting fracture network is represented by a graph with a set of nodes and edges or links. *Matlab* is used for the data processing; and for the geometric representation of the network, we employed a computational tool *Ucinet* (Borgatti et al., 2002). Networks resulting from this transformation are presented in Fig. 2. In this transformation of original fracture image into the construction of a graph, only the largest connected network is extracted from the image (see Figs. B4 and B5 in Appendix B), in graph theory it is named the largest component, this is, due to not all the fracture segments are connected among them. In Fig. B5, the nodes corresponding to the main component are labeled on the original image. In general, these resulting components or networks have an elongated structure

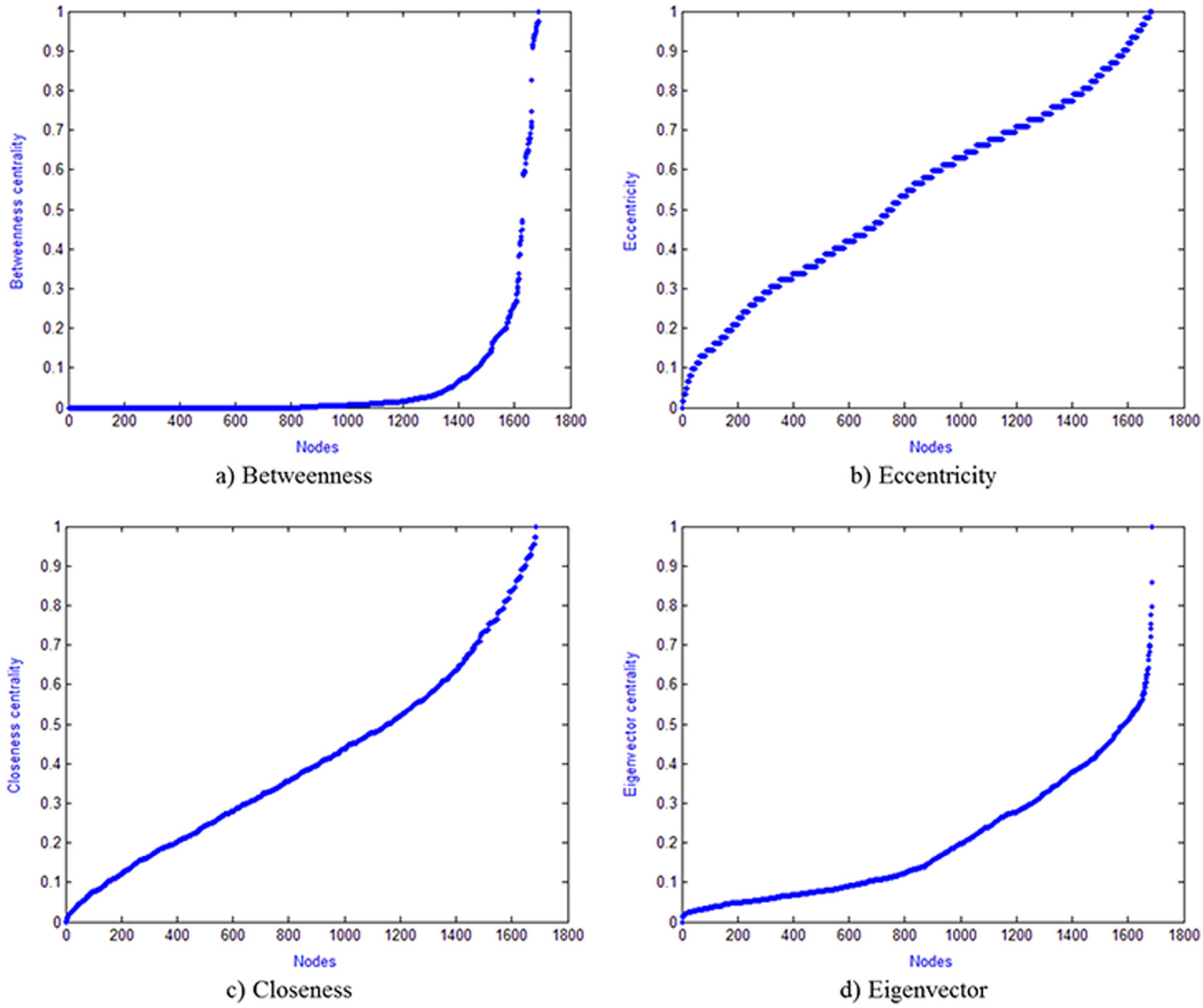

Fig. 3. Centrality measures applied to sample CH-2. Each graph indicates the behavior of a centrality measure, that is, betweenness, eccentricity, closeness and eigenvector for (a), (b), (c) and (d), respectively.The *x* axis displays the nodes in ascending order according to the resulting value of the metric applied (*y* axis).

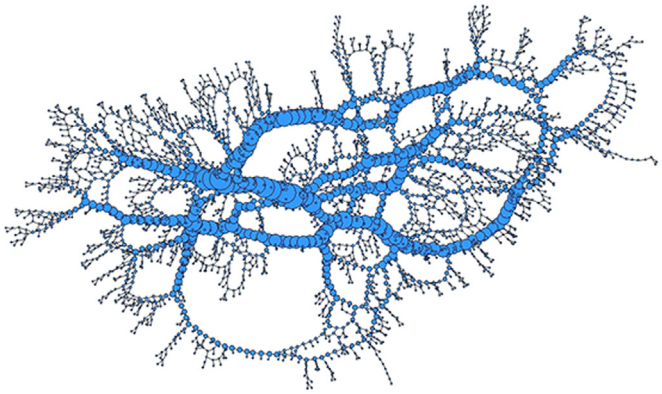

Fig. 4. Betweenness for sample JT-8 (see Fig. 2(b)). The magnitude is represented by the size of the nodes, where the lowest values are in the extreme of the branches while the highest values are in the central part of the structure (backbone) indicating the most important channels.

with many branches.

3.2. Metrics and topological classes in complex networks

For analyzing fracture networks, first we apply traditional statistical measures and then computing metrics that allow identifying the importance of nodes such as centrality measures. Later, in a second analysis we apply a topological approach for classifying fracture networks based on the local and global communicability, all of them are described in the following paragraphs.

Table 2
Results of connectivity and communicability indices in fracture networks.

Sample	*n*	*m*	Size (*n*/*m*)	*EE*(*G*)	$\sigma(G)$	*Comm*
JT- 6	633	728	0.869	1822.12	0.242	0.043
CH-2	1686	1905	0.885	4766.33	0.241	0.015
JT-3	779	887	0.878	2186.42	0.239	0.033
JT-8	3585	4183	0.857	10160.56	0.181	0.007
MM	1567	1996	0.785	4688.52	0.098	0.016

A basic centrality measure is the degree of a node (k_i) see Eq. (1) (Freeman, 1979) that adds up the links that connect to *i* node. Other sophisticated measures that also compute the centrality in the network utilizing distances among nodes are shown below

$$k_i = \sum_{j}^{n} A_{ji} \tag{1}$$

Closeness centrality is the inverse sum of the geodesic distances obtained from a given node to the rest of the nodes in the

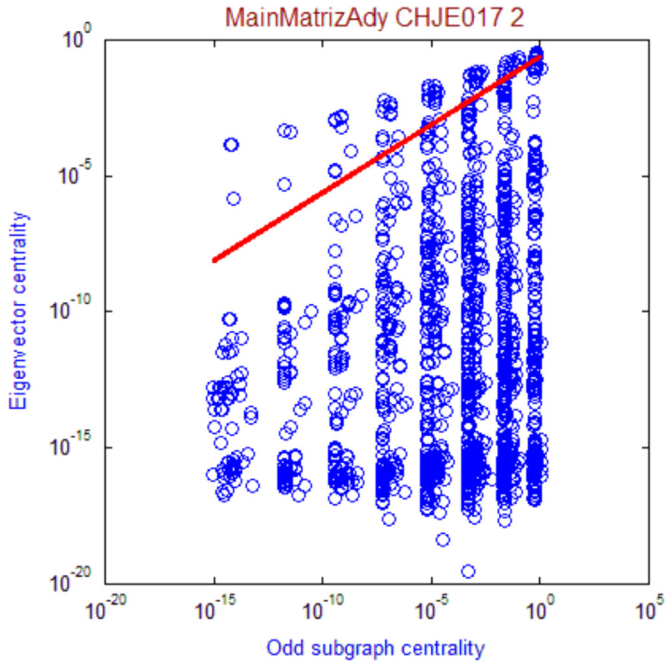

Fig. 5. Type of network class IV. In this graph, each circle represents the resulting correlation between local and global communicability of each node. Most nodes in each sample are correlated under the ideal line (local communicability is higher that the global communicability), that is, some neighborhoods of nodes are well communicated among them but at the same time they are few connected with other neighborhoods belonging to the fracture network. (For interpretation of the references to color in this figure, the reader is referred to the web version of this article.)

network (Sabidussi, 1966). Betweenness centrality counts the number of times where a node *i* falls on the geodesic paths among all the pairs of nodes (Freeman, 1979). Eigenvector centrality is based on the largest characteristic eigenvalue of the adjacency matrix (Bonacich, 1987). Eccentricity is defined as the shortest distance from a certain node to the farthest one in the network; in particular, the largest eccentricity is called the diameter of the network. A more detailed explanation of these metrics is given in Appendix A and references.

The communicability in the networks is analyzed by the Estrada index and denoted by $EE(G)$. This metric quantifies the amount of subgraphs in the network (see Eq. (A.8), Appendix A). Another measure of communicability described in Eq. (A.10) in Appendix A (Estrada, 2012) that defines the capacity to connect between pairs of nodes taking into account all the paths that connect to all nodes.

The correlation between local and global communicability in the network is computed using universal network classes defined in Estrada (2012). The local communicability for a given node is evaluated using the Estrada index considering odd closed path subgraphs; and eigenvector centrality is used to measure global communicability, combining these two variations of communicability four classes are defined. The first type of network (class I) is the homogeneous network or ideal network where the local communicability is representative of the global one, that is, all the nodes have the same degree in the whole network. The other three classes belong to heterogeneous networks where local communicability is not a good predictor of the global behavior (Estrada, 2007; Estrada and Hatano, 2007). Topologically, class II shows node neighborhoods separated by structural holes (neighborhoods with low communicability). Class III includes networks with highly connected nodes (central cores) surrounded by sparsely populated regions. Networks that combine both characteristics of class II and III are classified as class IV.

4. Results and discussions

A summary of the main characteristics of the fracture networks described previously is presented in Table 1. It includes the number of nodes (n) and edges (m), diameter (D), radius (r), clustering coefficient $\overline{C}$ and number of triangles (T) sorted by the number of nodes (633–3585). A ratio of network size is presented in the fourth column; it establishes a relation between the numbers of nodes and links, where a network with many links will have a value close to zero. In all our networks, the resulting values in the application of this metric are found between 0.78 and 0.88. The average clustering coefficient (0.0514) is relatively low, consistent with the existence of a low number of triangles. As a comparative example, this parameter takes values of 0.417 and 3.68 for problems associated with protein interaction and drug networks (Estrada, 2012), respectively, networks defined as small worlds (Watts and Strogatz, 1998). The last parameter indicates the intensity of fractures computed by the total number of links (fracture segments that connect the intersection of fracture traces) found in the whole sample; unlike the parameter M, m only includes the number of links belonging to the largest connected network. The length of each link or fracture segment was measured by the quantity of pixels, an example of length distribution taking the sample JT-6 is presented in Fig. B.6 in Appendix B.

4.1. Applying metrics to fracture networks

Unlike other networks, fracture networks have a low degree typically between 3 and 6, with the existence of many nodes of degree one corresponding to the extreme points of the segments of fractures (effect of sampling). In many networks (such as internet, protein, gene, social) this parameter usually varies from one to thousands or even millions of links.

To illustrate the relationships of the centrality measures (see Fig. 3) we use the network extracted from sample CH-2 (Fig. 2(d)). This fracture network has 1686 nodes shown in each subsection of Fig. 3 in ascending order with respect to the resulting values of each metric. Betweenness, eccentricity, closeness, and eigenvector centralities show similar patterns to all the fracture samples used (Figs. C.1–C.3 in Appendix C). In particular, for betweenness most nodes have a value less than 0.1, and a few nodes are found as the most important ones corresponding to the last one hundred nodes with value over 0.2 (Fig. 3(a)) thus indicating a direct dependence of fracture system size and the connectivity degree. In Fig. 4, we show the network backbone that comprises the nodes with the highest betweenness values (nodes represented by the largest circles). In a fluid flow context, the backbone would be the main structure for transporting any fluid. Eccentricity and closeness show an almost linear relation to each other associated to the elongated nature of the structures seen in all our network samples (Fig. 2(b) and (c)). Eigenvector centrality has a similar behavior to betweenness Fig. 3(d), with the difference that the first nodes in eigenvector take value over zero. For describing the flow efficiency considering the structure of the fracture network, we consider the connections among fractures in the rock by using the degree of nodes as is described in the next communicability indicators.

In Table 2, the results of communicability measures are presented. Fifth column shows the resulting values by the application of Estrada index ($EE(G)$), where the minimum and maximum values are 1822.12 and 10160.56 corresponding to fractures JT-6 and JT-8, respectively. As an example and in comparison with other complex networks (Estrada, 2012) the minimum and maximum real values for the trans-yeast and Internet networks are 3.589×10^4 and 6.174×10^{13} (considering the sum of odd and even

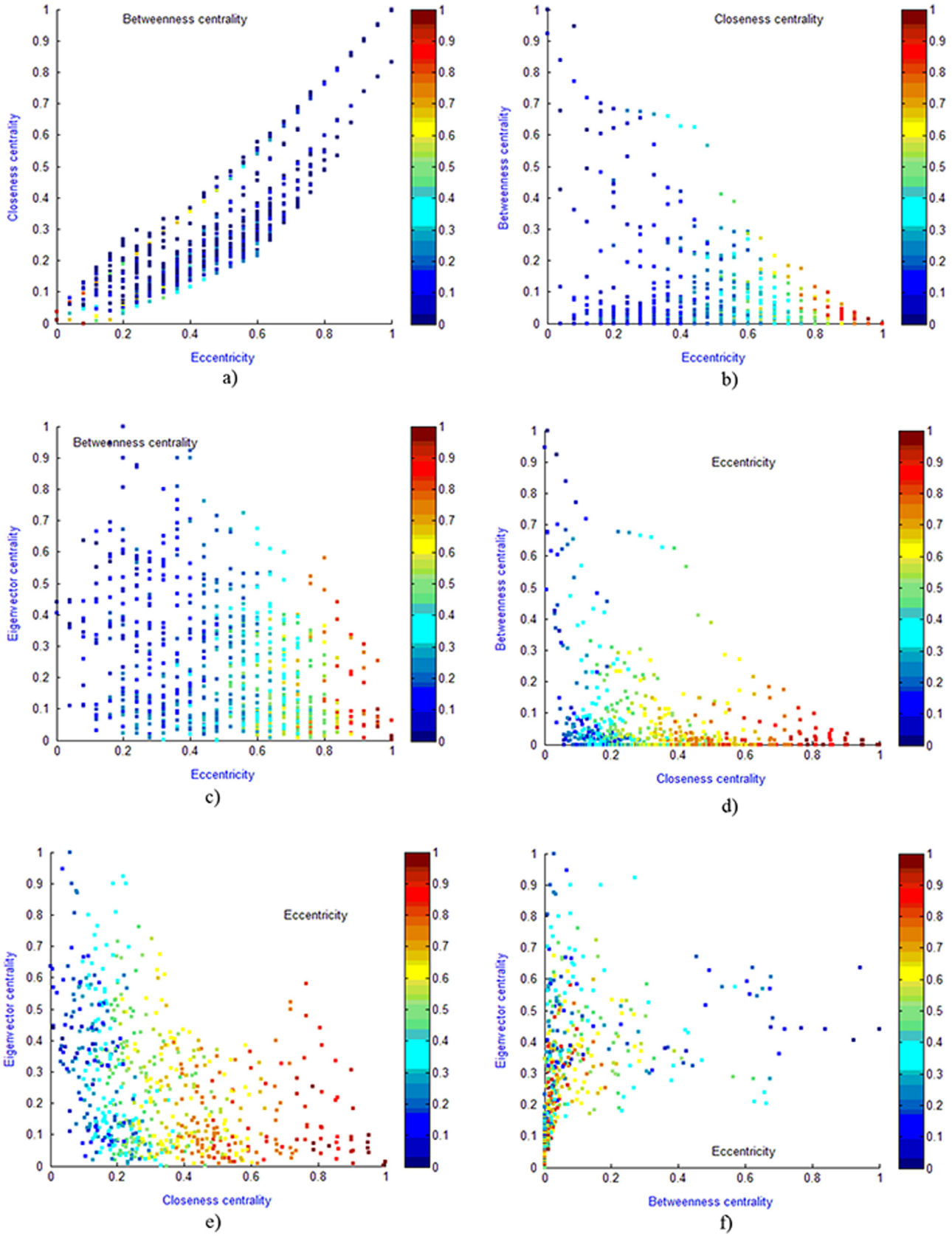

Fig. 6. Correlation among centrality measures. Each graphic compares three metrics using the sample JT-3 (Fig. 2(e)). The values of the metrics are indicated on the *x*, and *y* axes, and the third metric is expressed by the color intensity according to the normalized values (0-1). The different combinations of measures are shown by the subsections (a–f). (a) Eccentricity, closeness and betweenness; (b) Eccentricity, betweenness and closeness, (c) Eccentricity, eigenvector and betweenness, (d) Closeness, betweenness and eccentricity, (e) closeness, eigenvector and eccentricity, and (f) betweenness, eigenvector and eccentricity. (For interpretation of the references to color in this figure, the reader is referred to the web version of this article.)

paths). In our fracture network, the $EE(G)$ values are smaller than in those problems because of the low connectivity among nodes (Fig. 2), result characterized by the existence of many nodes that have one link and in consequence reduce the possibility of generating paths. A second measure is the *network invariability* $\sigma(G)$described in Eq. (A.7) in Appendix A. This index measures the heterogeneity of the degree (k_i) for all i in the network, and takes values between 0 and 1, where a value close to zero indicates a more regular network (same degree for all the nodes). This index is shown in Table 2 (sixth column) and comparing the heterogeneity with other networks where this metric has also been applied (Estrada et al., 2012); the fracture network values differ from the US power grid network (0.009) but the values are slightly similar to the human protein interaction network (0.283) that in average is 0.2 for fracture networks. Our networks present a low heterogeneity compared with other networks such as the Internet network (0.548), a paradigm of high heterogeneity. Note also that the values of $\sigma(G)$ are opposite to the values of $EE(G)$ in the following sense: for instance JT-8 has a maximum $EE(G)$ of 10160.56 being the network with more nodes in all our samples; however, it has one of the lowest values of $\sigma(G)$, 0.181. This result is an indicative that larger fracture networks (considering the ratio between number of nodes and links) have a tendency to "homogenize", that is, to maintain the same degree or number of links, which $\sigma(G)$ leads to values close to zero.

The results obtained applying the second measure of communicability (Eq. (A.10) in Appendix A) are displayed in the last column (*comm*) in Table 2. In general, the values are less than 0.05, indicating low communicability in these samples but slight variations among them due to the different ratios (n/m). In the next section, these indexes are used in order to define a topological class for fracture networks.

4.2. Identifying a topological class for fracture networks

According to the description of the four topological classes presented in Section 3, we correlate local and global communicability in the network to identify the universal network class to which belong the fracture networks, and we obtained that our fracture networks belong to class IV. An example is shown in Fig. 5 (sample CH-2), where the red line is the theoretical correlation between subgraph centrality (x axis) and eigenvector centrality (y axis) (Estrada, 2007), and this line also characterizes a homogeneous network (nodes with the same degree). Note that a mixture of positive and negative deviations around the expected theoretical behavior exists. This pattern is illustrated in Fig. 2(b), where it is observed that local neighborhoods are highly connected but the presence of holes produces low global communicability in the whole network. Similar results for the rest of the fracture network samples are presented in Appendix D. In the next section, the centrality measures are used to identify correlations among them and in order to find patterns in fracture networks.

4.3. Comparison among centrality measures

Using sample JT-3 (Fig. 2(e)) as a typical example, six comparative graphics of the resulting characteristics are presented in Fig. 6. Each graph displays three normalized centrality measures and the relations are explained as follows. In Fig. 6(a) is shown a positive correlation between eccentricity and closeness centrality indicating that the value of the shortest distance of a given node to the farthest one has the same behavior as the average distance obtained of one given node to all the nodes of the whole network, this pattern is also shown in Fig. 6(b). Recall that we are using the inverse form for closeness centrality (see Eq. (A.4)).

Note that he greatest betweenness centrality is located on left bottom in Fig. 6(a) (values on x between 0 and 0.2). These nodes are interpreted as bottlenecks since the shortest paths pass through them. In addition, the nodes with the lowest closeness centrality and eccentricity have the greatest betweenness values (called central nodes) and are displayed in Fig. 6(b) and (d) on the left side in a triangular distribution region.

Eccentricity in Fig. 6(d) shows a large variability and has a rapid decay in the range between 0 and 0.4 (on x axis). Nodes with values less than 0.4 belong to the backbone of the network, nodes with values greater than 0.4 form part of the branches of the network. The comparison between eigenvector centrality and eccentricity in Fig. 6(c) does not show a definite pattern. However, we found a relationship between eigenvector and closeness centrality in Fig. 6(e); where nodes with the largest closeness centrality (extreme nodes) and nodes with the smallest closeness centrality (central nodes) are highly connected. This is observed in the largest values on y axis if Fig. 6(e) indicating that locally some extreme nodes form part of some highly connected branches, and of course the central nodes as well. These results are consistent with the structures displayed in Fig. 2.

In Fig. 6(c), the lowest betweenness values prevail over almost all the range on the x axis (values between 0 and 0.8). Eccentricity in most nodes is less than 0.6 indicating that our fracture networks have in general short paths between any pair of nodes, and a few are far away from the rest. Observe that in Fig. 6(e) most of the nodes are concentrated in the region where the closeness index is less than 0.8; however, there is no relationship with eigenvector centrality.

The relationship between eigenvector and betweenness is shown in Fig. 6(f), where it displays high concentration of nodes in the range between 0 and 0.2 (on x axis) indicating that these nodes belong to the network branches; and few nodes with values over 0.2 belong to the backbone. Also in Fig. 6(f), the greatest eccentricities are concentrated in the range 0–0.2 on x axis. The patterns found in Fig. 6 are similar to the rest of samples studied in this work (see Appendix E). In general, the samples show a strong dependence of their topological indices on the quantity of nodes and links.

In summary, topologically we can conclude that fracture networks are structures with low heterogeneity in terms of global connection. With respect to the communicability, nodes with high importance in the whole network have the lowest closeness centrality (Fig. 6(d)). This result agrees with observations on other networks (Estrada, 2012), where a negative correlation between these two indices is typical.

5. Conclusions

According to our analysis, fracture networks belong topologically to class IV characterized by the presence of holes surrounded by neighborhoods of connected nodes. The node degree for this kind of networks is at most 6 in all the fracture samples. A positive linear correlation exists between closeness centrality and eccentricity due to the characteristic elongated pattern found in the networks analyzed. However, an opposite correlation exists between closeness centrality and betweenness centrality as is shown in Fig. 6(b) and (d), and this behavior is also identified between eccentricity and betweenness centrality. It is observed that the farness between two nodes results in a low betweenness centrality since central nodes are located, in most fracture samples, on the main stem or backbone of the fracture network. Eigenvector centrality has a large variability with respect to other metrics except for betweenness where a tendency prevails along the mean value of eigenvalue centrality as was shown in

subsection (f) in Fig. 6. In addition, the narrow range of node degree forces these networks to possess low heterogeneity, and therefore low communicability.

Acknowledgments

JXVH acknowledges partial support from PAPIIT-UNAM Project IA1012015. We thank Dr. Luis G. Velasquillo, Dr. Diego Del Castillo and Dr. Ernesto Estrada for fruitful discussions and insights.

Appendix A. Description of metrics

In this appendix, definitions and formulations of the metrics used in this work are presented. The first ones correspond to four centrality measures and the last ones to communicability measures.

Betweenness centrality

This measure was proposed initially by (Anthonisse, 1971), and later by (Freeman, 1977). These authors define centrality $C_B(i)$ as the ratio between ρ_{st}(i) and ρ_{st}, i.e., the number of times in which a node i falls on the geodesic path between the nodes s and t, and the number of shortest paths between the nodes s and t, respectively. The formula for computing betweenness of a certain node i is presented in Eq. (A.1). It measures the potential for controlling the communication of a network. An improved version of this centrality index is defined in (Brandes, 2001) and is expressed in (A.2), where ρ_{st}(i) takes the value of $\rho_{si.}\ \rho_{it}$ if the shortest paths between s and t pass through the node i, otherwise takes zero. d_G (s,t) is the shortest distance between the nodes s and t. A high centrality score indicates that a node can be reached by other nodes on short paths

$$C_B(i) = \sum_{s \neq i \neq t} \frac{\sigma_{st}(i)}{\sigma_{st}}, \cdot \forall\, s, t \in V \tag{A.1}$$

$$\sigma_{st}(i) = \begin{cases} 0 \text{ if} d_G(s,t) < d_G(s,i) + d_G(i,t) \\ \sigma_{si.}\ \sigma_{it} \qquad \text{otherwise} \end{cases} \tag{A.2}$$

Closeness centrality: This measure adds up the inverse of the sum the distances of a node to all other nodes in the network, which is expressed by $C_C(v)$ in Eq. (A.3) (Sabidussi, 1966). For a node v, it measures the inverse of the sum of the geodesic distances from a v node to a t node, for all $t \epsilon V$. An inverse form of the closeness centrality is described in Eq. (A.4), and it is used in this work

$$C_C(v) = \frac{1}{\sum_{t \in V} d_G(v,t)} \tag{A.3}$$

$$C_F(v) = \frac{\sum_{t \in V} d_G(v,t)}{n-1} \tag{A.4}$$

Eigenvector centrality: The function of this measure is to find the most central nodes (Bonacich, 1972; Bonacich, 1987), i.e. those with the smallest farness from others in terms of the global structure of the network. The assumption is that each node's centrality is the sum of the centrality values of the nodes that it is connected to, and a node has high score if connected to many nodes that are themselves well connected. The centrality matrix obtained is an eigenvector of the adjacency matrix such that all of its elements are positive. Eigenvector centrality is defined as the eigenvector of **A** with the largest eigenvalue as in (A.5), where v is the eigenvector for the maximum eigenvalue $\lambda_{\max}(A)$ of the adjacency matrix **A**.

$$C_E(i) = \frac{1}{\lambda_{max}(A)} \sum_{j}^{n} a_{ji} v_j \tag{A.5}$$

Eccentricity

This measure represented by $e(i)$ in Eq. (A.6). It computes for a node i the number of steps that are necessary to reach the t farthest node (Sabidussi, 1966) in the whole network. This measure also considers the geodesic path (or the shortest path) between nodes, where the largest geodesic path in the network is its diameter. $d_G(i,t)$ indicates the shortest path of a node i to the node t, and $\max(d_G(i,t))$ represents the largest geodesic path identified from the list of geodesic paths generated from node i to t node, for $t \epsilon V$

$$e(i) = \max(d_G(i,t)), \cdot \forall\, i, t \in V \tag{A.6}$$

Invariability index in the network

This index expressed by Estrada (2010b) represents the normalized degree heterogeneity in a network by considering all pairs of nodes that are connected to and is presented in Eq. (A.7). The index varies from zero to 1, where minimum is obtained for any regular network and the maximum is obtained for type star networks. Where k_i and k_j are the degrees of the nodes i and j

$$\rho(G) = \frac{1}{n - 2\sqrt{n-1}} \sum_{i,j \in E} \left(\frac{1}{\sqrt{k_i}} - \frac{1}{\sqrt{k_j}} \right)^2 \tag{A.7}$$

Estrada index

This topological index proposed by Estrada (2000) measures the invariability of a network by accounting for all the subgraphs in a global way. This index was initially used in the folding of proteins, and later De la Peña et al. (2007) renamed it as “index Estrada” of a graph. The formula is presented in Eq. (A.8), where A is the adjacency matrix associated to the graph G

$$EE(G) = tr(e^A) \tag{A.8}$$

Communicability

Another communicability index accounts for all the channels of communication between nodes giving more weight to the shortest paths that connect them is presented in Eq. (A.10) which eliminates the $EE(G)$ from the exponential matrix (Eq. (A.9)) defined by (Estrada, 2012)

$$G' = e^A \tag{A.9}$$

$$Comm = \frac{2^*\left(\sum G' - tr(e^A)\right)}{n^*(n-1)} \tag{A.10}$$

Clustering Coefficient: This index defines the number of triangles connected to a certain node i, $|C_3(i)|$, divided by the number of triples from this node (Watts and Strogatz, 1998). This definition is formulated in Eq. (A.11), where k_i is the node degree i, and the clustering coefficient average is expressed in (A.12)

$$C_i = \frac{2^*|C_3(i)|}{k_i(k_i-1)} \tag{A.11}$$

$$\overline{C} = \frac{1}{n}\sum_{i=1}^{n} C_i \tag{A.12}$$

Appendix B. Original sketches of fractures in rocks

See Figs. B.1–B.6

Appendix C

See Figs. C.1–C.3

The three figures below exhibit behaviors of the respective centrality measures, closeness, betweenness and eigenvector, including in each figure the four samples used.

Fig. B.1. Sample CH-2.

Appendix D. Topology of classes for fracture network

See Fig. D.1

In this figure, results of applying the local and global communicability measures for classifying the fracture networks are presented for four samples.

Appendix E. Comparative graphics of centrality measures

See Figs. E.1–E.3

In this appendix, three figures are shown where each of them indicates a different comparative of three centrality measures presented for the four fracture network samples.

Fig.B.3. Sample JT-8.

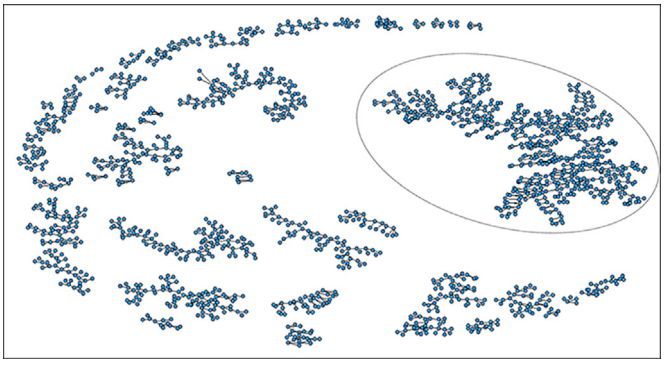

Fig. B.4. Networks obtained of sample JT-6 (Fig. 1), the nodes (circles) indicate the intersection or extreme points of the fracture segments, and the links are the connections among intersections or extreme points. The enclosed network is the largest connected network (component with more nodes), and it is used in our analysis.

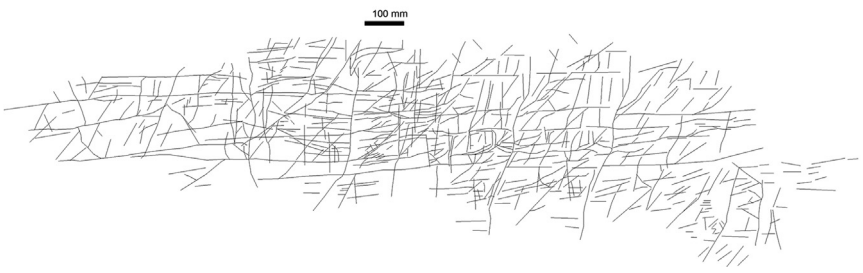

Fig. B.2. Sample JT-3.

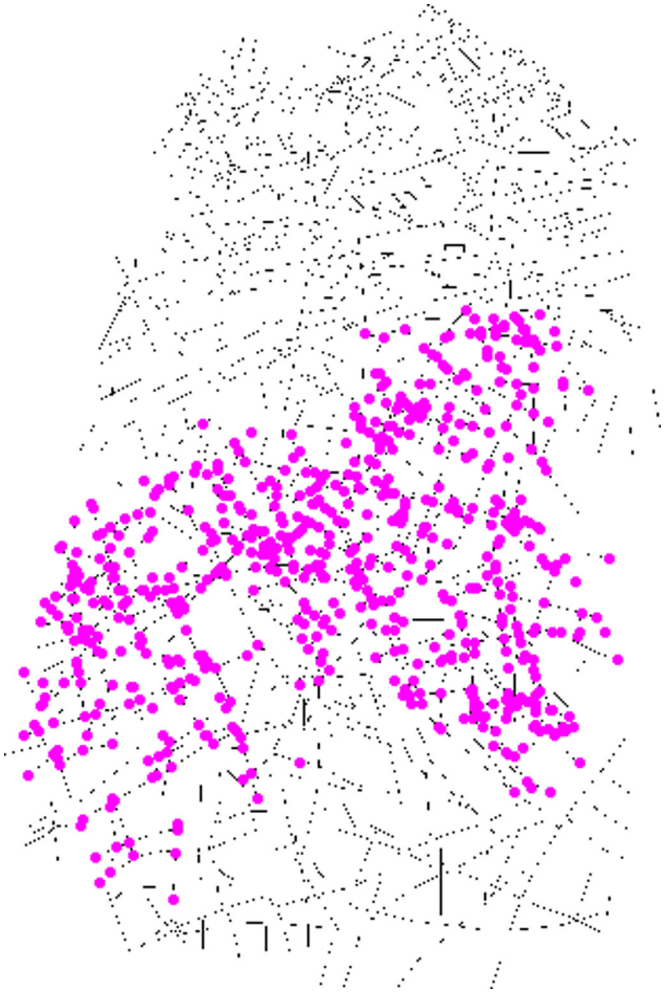

Fig. B.5. The largest connected network in sample JT-6. The labels in circles represent the nodes or intersections of fracture traces that form the main component. In picture, the traces look like discontinue lines however if we look very closely they are solid lines.

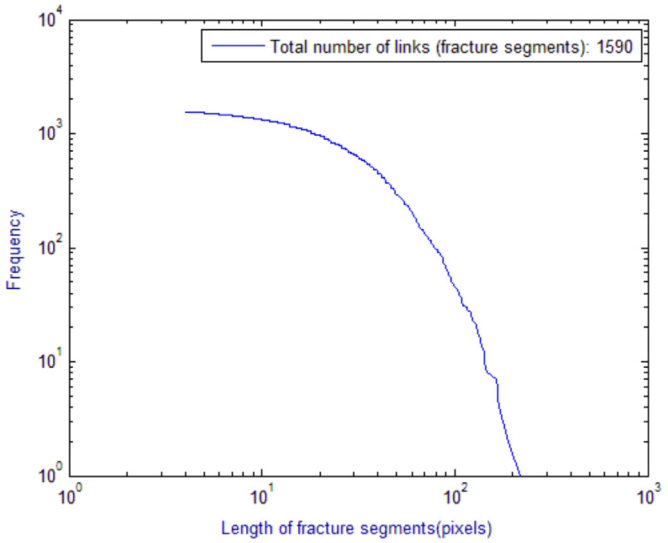

Fig. B.6. Length distribution of fracture segments from sample JT-6 (see Fig. 1). In this picture all the links (trace of fracture) are measured by the quantity of pixels; where *x* axis indicates the length of the segments, and *y* axis represents the frequency. The behavior of this distribution is similar to the rest of the samples of fractures.

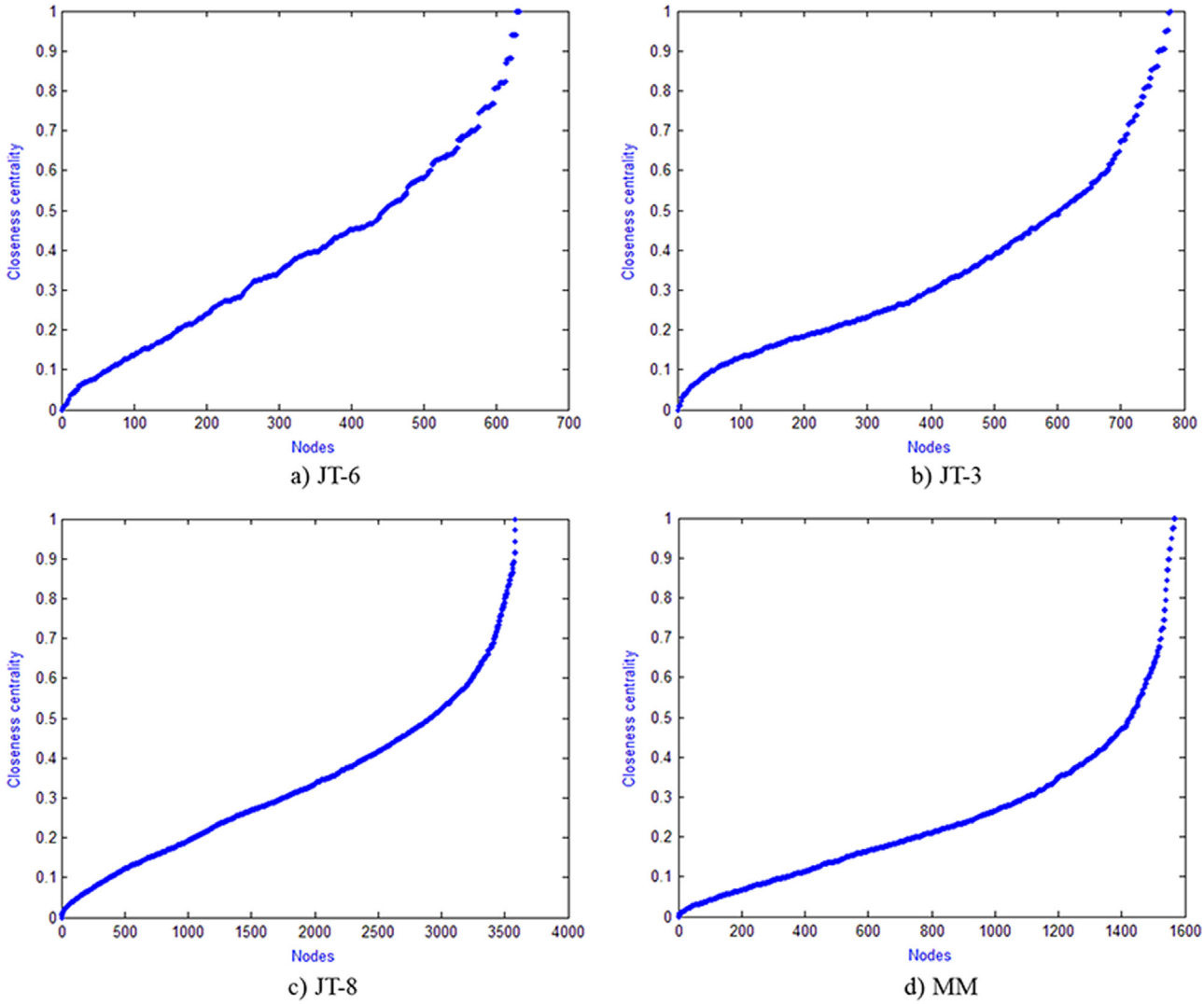

Fig. C.1. Closeness centrality. Each graph presents the normalized closeness values in ascending order for four samples. This measure indicates the average closeness to all the nodes. Observe almost an increasing lineal variation in the values for sample JT-6 and a curved behavior for JT-3, JT-8 and MM.

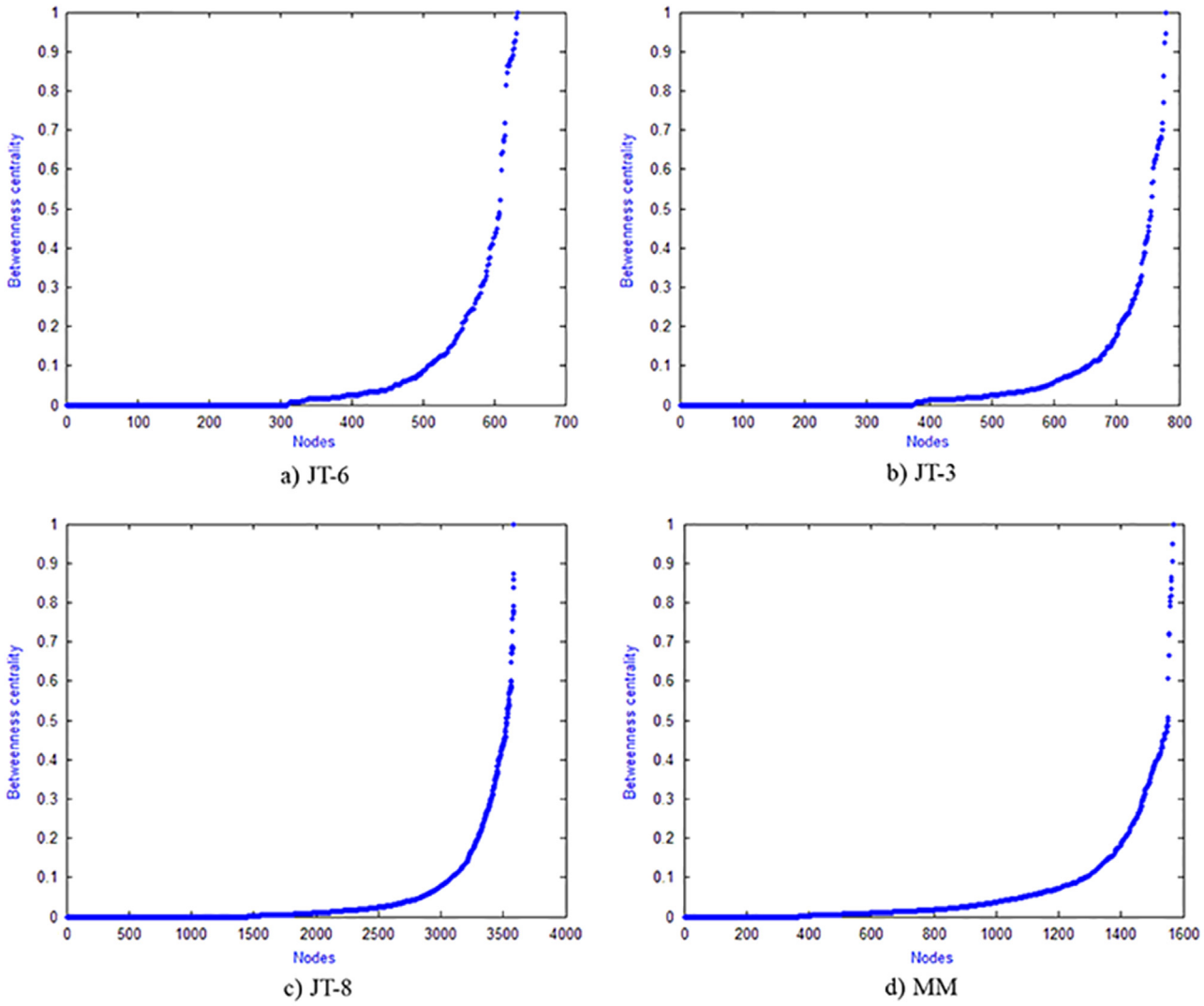

Fig. C.2. Betweenness centrality. Each graph displays the normalized betweenness values in ascending order, where approximately 50% of the nodes (intersection of fractures) in every figure have values zero (they indicate extreme points in the fractures networks), and some few nodes have high betweenness values (it can be seen at the end of the line).

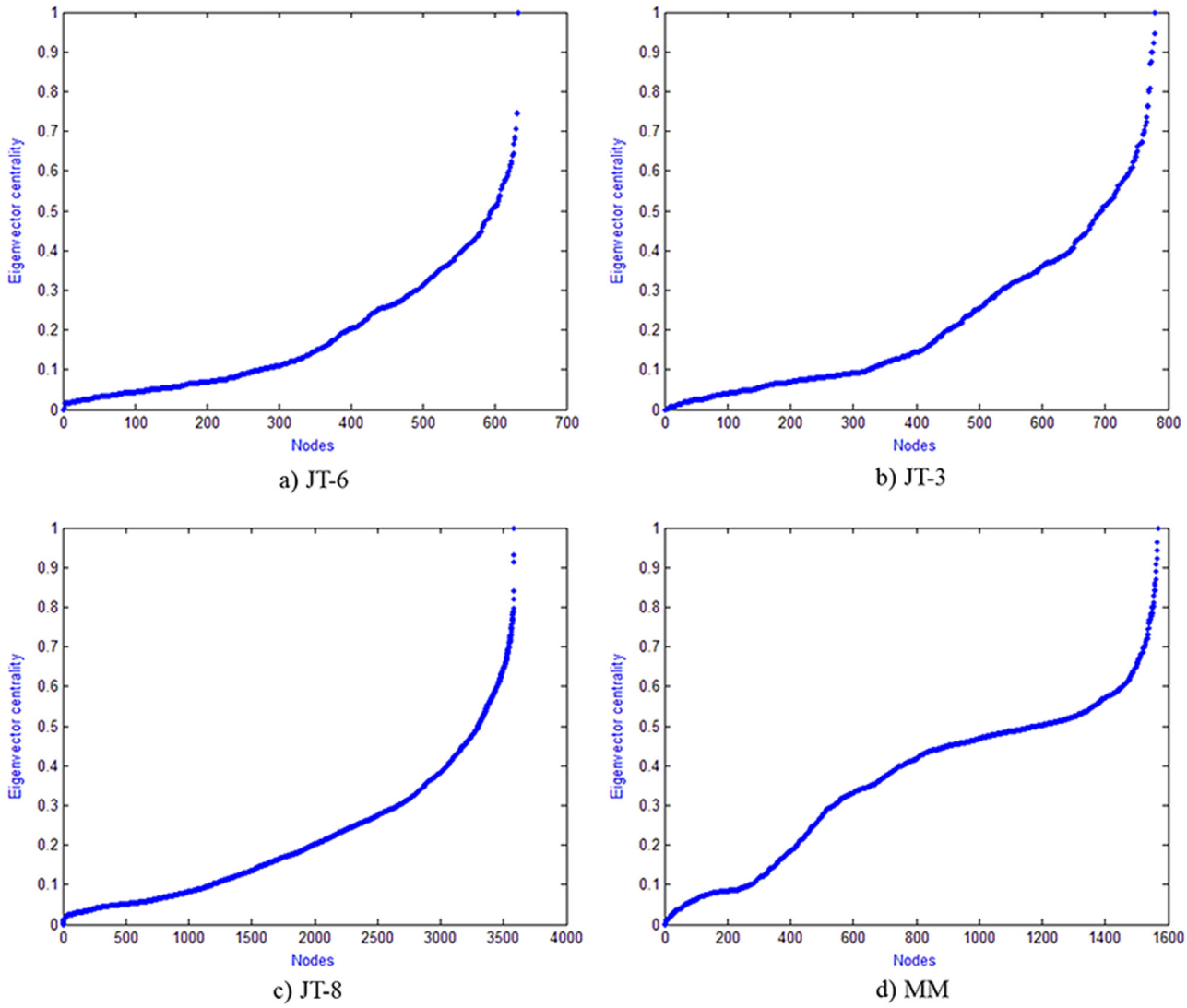

Fig. C.3. Eigenvector centrality. Each graph presents sorted and normalized eigenvalue values in ascending for each sample. Similar patterns are found in (a), (b) and (d) where a curved line indicates that the values in most nodes are lower than 0.5 and some few nodes have a high value; however, in sample MM a wave line is displayed pointing out some nodes have similar value of eigenvector centrality.

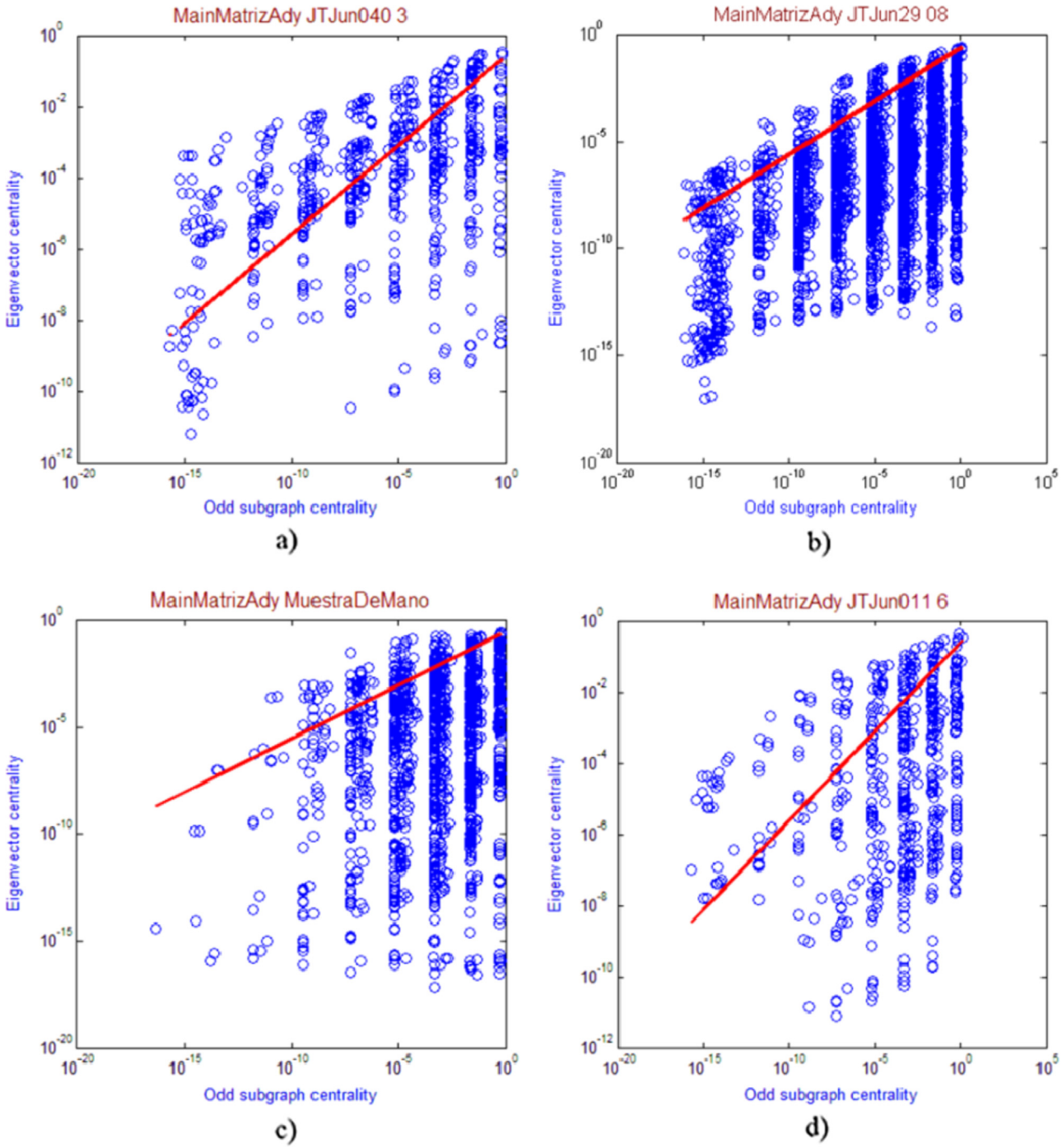

Fig. D. 1. Type IV class for fracture networks in rocks. In these figures, the line shows the behavior of a homogenous network. Each circle represents the resulting correlation between local and global communicability of each node. Most nodes in each sample are correlated under the ideal line that indicates that local communicability is higher than global communicability. (For interpretation of the references to color in this figure legend, the reader is referred to the web version of this article.)

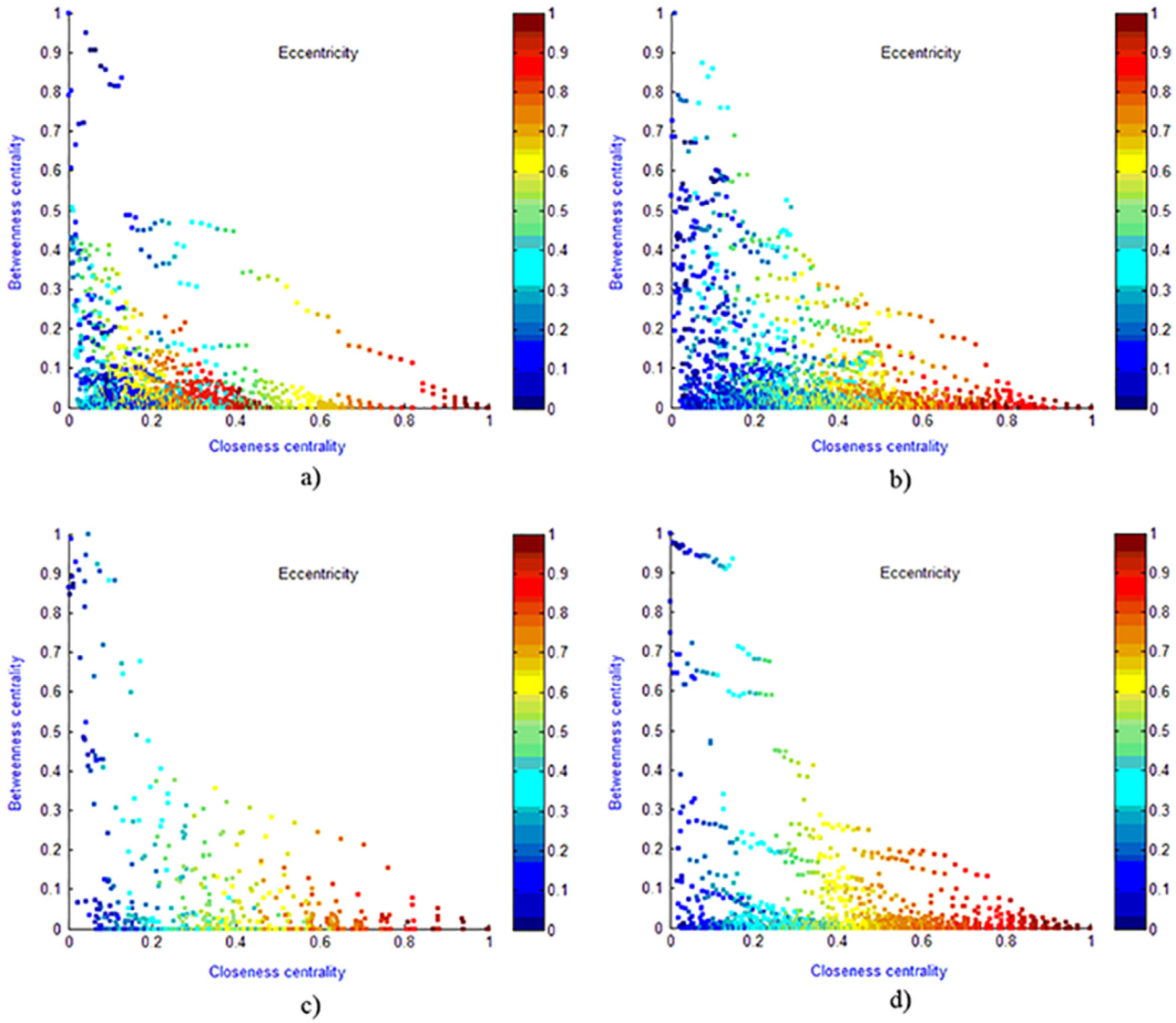

Fig. E.1. Closeness centrality (*x* axis) vs betweenness centrality (*y* axis) vs eccentricity (colorbar): (a) fracture MM, (b) fracture JT-8, (c) fracture JT-6, and (d) fracture CH-2.

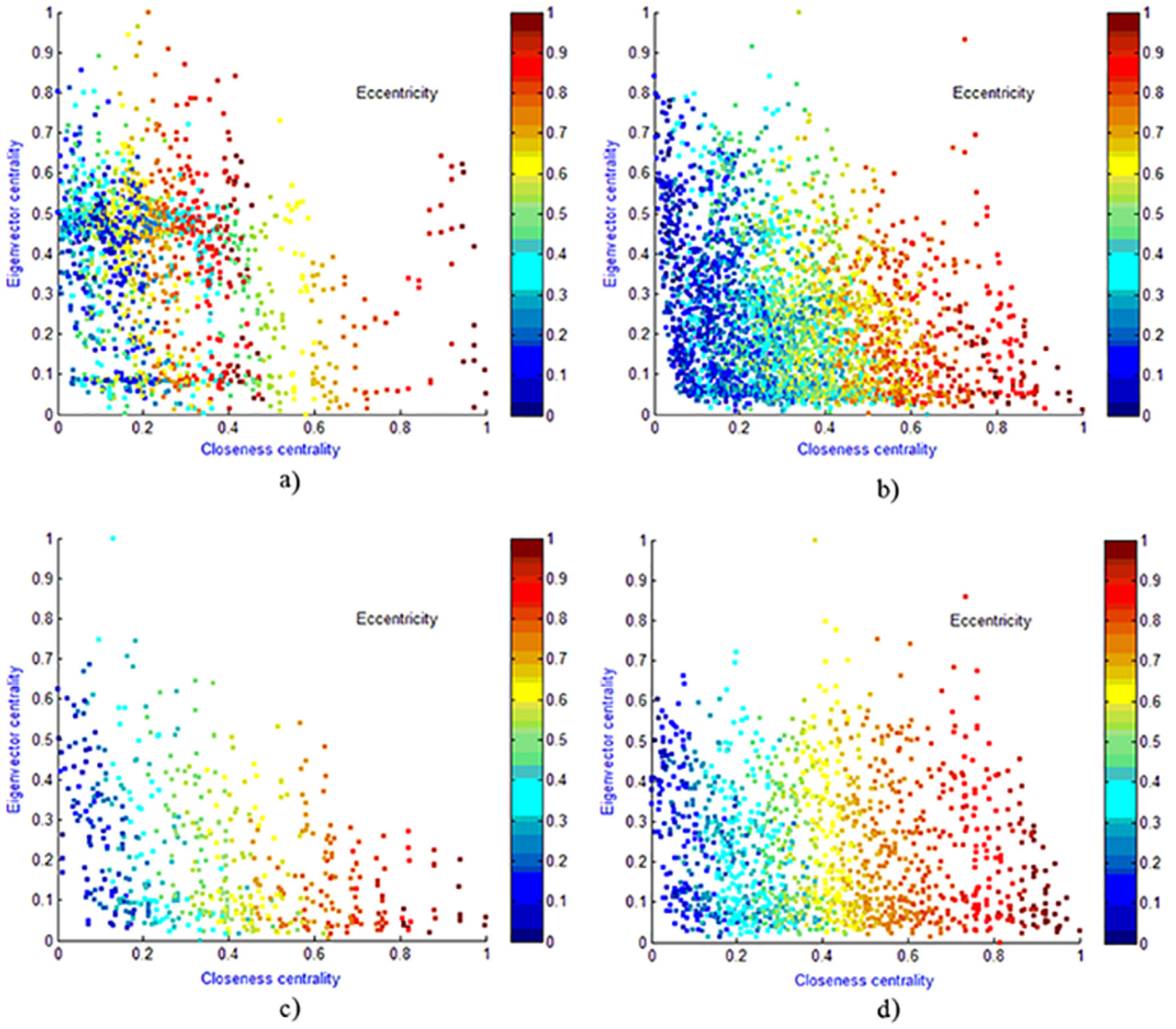

Fig. E.2. Closeness centrality (x axis) vs eigenvector centrality (y axis) vs eccentricity (colorbar) for five samples: (a) fracture MM, (b) fracture JT-8, (c) fracture JT-6, and (d) fracture CH-2.

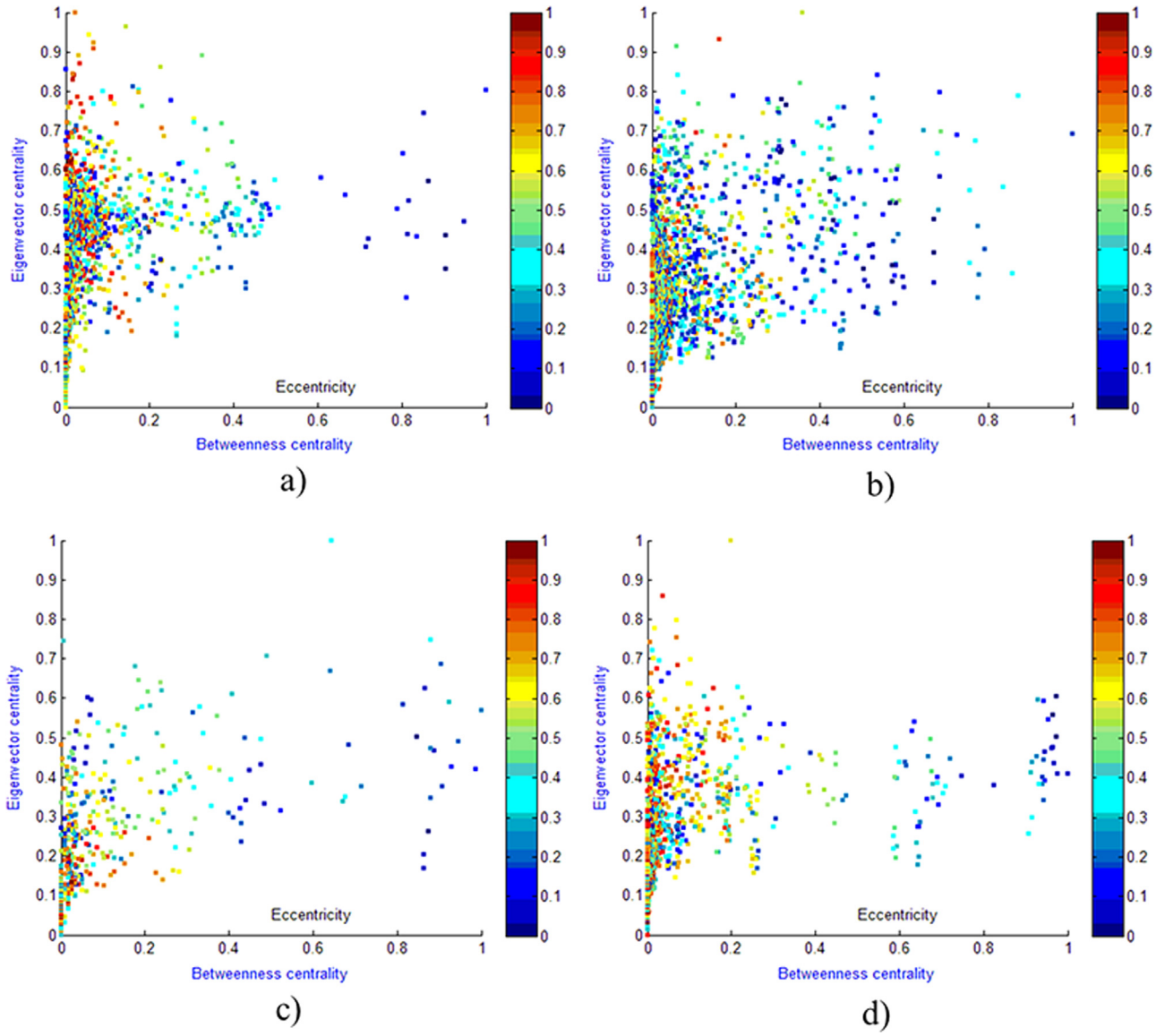

Fig. E.3. Betweenness centrality (x axis) vs eigenvector centrality (y axis) vs eccentricity (colorbar) for five samples: (a) fracture MM, (b) fracture JT-8, (c) fracture JT-6, and (d) fracture CH-2.

References

Andresen, C.A., Hansen, A., Le Goc, R., Davy, P., Hope, S.M., 2013. Topology of fracture networks. Interdiscip. Phys. 1, 7. http://dx.doi.org/10.3389/fphy.2013.00007.

Anthonisse, J.M., 1971. The rush in a graph. Mathematisch Centrum. Amsterdam (mimeographed).

Baker, R.O., Kuppe F., 2000. Reservoir Characterization for Naturally Fractured Reservoirs. In: Proceedings of SPE Annual Technical Conference and Exhibition, Paper SPE 63286. Dallas, Texas.

Berkowitz, B., 2002. Characterizing flow and transport in fractured geological media: a review. Adv. Water Resour. 25 (8–12), 861–884.

Bogatkov, D., Babadagli, T., 2007. Characterization of Fracture Network System of the Midale Field. Paper 2007-031, CIM 58th Annual Tech. Meet., Canadian International Petroleum Conf. Calgary, Canada.

Bonacich, P., 1972. Factoring and weighting approaches to status scores and clique identification. J. Math. Sociol. 2, 113–120.

Bonacich, P., 1987. Power and centrality: A family of measures. Am. J. Sociol. 92 (5), 1170–1182.

Borgatti, S.P., Everett, M.G., Freeman, L.C., 2002. Ucinet for Windows: Software for Social Network Analysis. Analytic Technologies, Harvard, MA.

Brandes, U., 2001. A faster algorithm for betweenness centrality. J. Math. Sociol. 25 (2), 163–177.

Bour, O., Davy, P., 1998. On the connectivity of three-dimensional fault networks. Water Resour. Res. 34 (10), 2611–2622.

Cacas, M.C., Ledoux, E., Marsily, G., Tillie, B., 1990. Modeling fracture flow with a stochastic discrete fracture network: calibration and validation. Water Resour. Res. 26 (3), 479–489.

Caine, J.S., Evans, J.P., Forster, C.B., 1996. Fault zone architecture and permeability structure. Geology 24, 1025–1028.

De la Peña, J.A., Gutman, I., Rada, J., 2007. Linear Algebra Appl. 427, 70–76. http://dx.doi.org/10.1016/j.laa.2007.06.020.

Dershowitz, W.S., Herda, H.H., 1992. Interpretation of fracture spacing and intensity. Am. Rock Mech. Assoc. The 33th USRMS, Santa Fe, New Mexico.

Escuder-Viruete, J., Carbonell, R., Martí, D., Jurado, M.J., Pérez-Estaún, A., 2003. Architecture of fault zones determined from outcrop, cores, 3-D seismic tomography andgeostatistical modelling: example from the Albalá granitic pluton, SW Iberian Variscan massif. Tectonophysics 361, 97–120.

Estrada, E., 2000. Characterization of 3D molecular structure. Chem. Phys. Lett. 319, 713–718.

Estrada, E., 2007. Topological structural classes of complex networks. Phys. Rev. E 75, 016103.

Estrada, E., 2010a. Quantifying network heterogeneity. Phys. Rev. E 82, 066102.

Estrada, E., 2010b. A vibrational approach to node centrality and vulnerability in complex networks. Physica A 389, 3648–3660.

Estrada, E., 2012. The Structure of Complex Networks. Theory and application. Oxford University Press, Oxford.

Estrada, E., Hatano, N., 2007. Statistical-mechanical approach to subgraph centrality in complex networks. Chem. Phys. Lett. 439, 247–251.

Estrada, E., Hatano, N., Benzi, M., 2012. The physics of communicability in complex. Phys. Rep. 514. http://dx.doi.org/10.1016/j.physrep.2012.01.006.

Freeman, L.C., 1977. A set of measures of centrality based on betweenness. Sociometry 40 (1), 35–41.

Ghaffar, H.O., Nasseri, M.H.B., Young, R.P., 2012. Fluid Flow Complexity in Fracture

Network, Analysis with Graph Theory and LBM. arXiv:1107.4918 [cs.CE].
Hakami, E., Larsson, E., 1996. Aperture measurements and flow experiments on a single natural fracture. Int. J. Rock. Mech. Min. Sci. Geomech. Abstr. 33 (4), 395–404.
Han, J.J., Lee, T.H., Sung, W.M., 2013. Analysis of Oil Production Behavior for the Fractured Basement Reservoir Using Hybrid Discrete Fractured. Netw. Approach. Adv. Pet. Explor. Dev. 5 (1), 63–70. http://dx.doi.org/10.3968/j.aped.1925543820130501.1068.
Hansford, J., Fisher, Q., 2009. The Influence of Fracture Closure from Petroleum Production from Naturally Fractured Reservoirs: A Simulation Modelling Approach.
Hardebol, N.J., Bertotti, G., 2013. DigiFract: A software and data model implementation for flexible acquisition and processing of fracture data from outcrops. Computer & Geosciences 54, 326–336. http://dx.doi.org/10.1016/j.cageo.2012.10.021.
Hitchmough, A.M., Riley, M.S., Herbert, A.W., Tellam, J.H., 2007. Estimating the hydraulic properties of the fracture network in a sandstone aquifer. J. Contam. Hydrol. 93, 38–57.
Jafari, A., Babadagli, T., 2012. Estimation of equivalent fracture network permeability using fractal and statistical network properties. J. Pet. Sci. Eng. 92–93, 110–123. http://dx.doi.org/10.1016/j.petrol.2012.06.007.
Koike, K., Kubo, T., Liu, C., Masoud, A., Amano, K., Kurihara, A., Matsuoka, T., Lanyon, B., 2015. 3D geostatistical modeling of fracture system in a granitic massif to characterize hydraulic properties and fracture distribution. Tectonophysics 660, 1–16. http://dx.doi.org/10.1016/j.tecto.2015.06.008.
Lee, C.C., Lee, C.H., Yeh, H.F., Lin, H.I., 2011. Modeling spatial fracture intensity as a control on flow in fractured rock. Environ. Earth Sci. 63 (6), 1199–1211. http://dx.doi.org/10.1007/s12665-010-0794-x.
Lyman, G.I., 2003. Stereological and other methods applied to rock joint size estimation – does Crofton's theorem apply. Math. Geol. J. 35 (1), Kluwer Academic Publisher, 9–23.
Narr, W., Schechter, D.S., Thompson, L.B., 2006. Naturally Fractured Reservoir Characterization. Society of Petroleum Engineers, Richardson, Texas.
Newman, M.E.J., 2003. The structure and function of complex networks. SIAM Rev. 45 (2), 167–256.
Newman, M.E.J., 2010. Networks: An Introduction. Oxford University Press, Oxford.
Rouleau, A., Gale, J.E., 1985. Statistical characterization of the fracture system in the Stripa granite, Sweden. Int. J. Rock. Mech. Min. Sci. Geomech. Abstr. 22 (6), 353–367.
Sabidussi, G., 1966. The centrality index of a graph. Psychometrika 31, 581–603.
Sanderson, D.J., Nixon, C.W., 2015. The use of topology in fracture network characterization. J. Struct. Geol. 72, 55–66. http://dx.doi.org/10.1016/j.jsg.2015.01.005.
Santiago, E., Romero-Salcedo, M., Velasco-Hernández, J.X., 2012. An integrated strategy for analyzing flow conductivity of fractures in a naturally fractured reservoir using a complex network metric, advances in computational intelligence. MICAI 2012, Lecture Notes in Computer Science. Vol. 76302013, pp 350–361.
Santiago, E., Velasco-Hernández, J.X., Romero-Salcedo, M., 2014. A methodology for the characterization of flow conductivity through the identification of communities in samples of fractured rocks. Expert Syst. Appl. 41 (3), 811–820.
Sarda, S., Jeannin, L., Basquet, R., Bourbiaux, B., 2002. Hydraulic characterization of fractured reservoirs: simulation on discrete fracture models. SPEREE 5 (2), 154–162, SPE-77300-PA.
Sarkar, S., Toksöz, M.N., Burns, D.R., 2004. Fluid Flow Simulation in Fractured Reservoirs, Research Report. Earth Resources Laboratory, Department of Earth, Atmospheric, and Planetary Sciences, Massachusetts Institute of Technology, USA http://hdl.handle.net/1721.1/68616.
Seetal, P., Natarajan, N., 2010. Image Segmentation for rock fractures based on ARMA model. Int. J. Eng. Sci. Technol. 2 (5), 1155–1159.
Smith, I., Schwartz, F.W., 1984. An analysis of the influence of fracture geometry on mass transport in fractured media. Water Resour. Res. 20 (9), 1241–1252. http://dx.doi.org/10.1029/WR020i009p01241.
Voeckler, H., Allen, D.M., 2012. Estimating regional scale fractured bedrock hydraulic conductivity using discrete fracture network (DFN) modeling. Hydrogeol. J. 20, 1081–1100.
Wang, S.Y., Sloan, S.W., Huang, M.L., 2011. Numerical study of failure mechanism of serial and parallel rock pillars. Rock Mech. Rock Eng. 44 (2), 179–198.
Watts, D.J., Strogatz, S., 1998. Collective dynamics of 'small-world' networks. Nature 393, 440–442. http://dx.doi.org/10.1038/30918.
Witte, J., Bonora, M., Carbone, C., Oncken, O., 2012. Fracture evolution in oil-producing sills of the Rio Grande Valley, northern Neuquen Basin, Argentina. AAPG Bull. 96 (7), 1253–1277. http://dx.doi.org/10.1306/10181110152.
Yang, G., Myer, L.R., Brown, S.R., Cook, N.G.W., 1995. Microscopic analysis of macroscopic transport properties of single natural fractures using graph theory algorithms. Geophys. Res. Lett. 22 (11), 1429–1432. http://dx.doi.org/10.1029/95GL01498.